RSC Advances

PAPER

View Article Online
View Journal | View Issue

Cite this: *RSC Adv.*, 2026, **16**, 8720

Exploring the anti-virulent potential of pyridine derivatives against *Vibrio cholerae*

Anusree Sajeevan,[a] Deepthi Joseph Andrew,[a] Vignesh Balaraman,[b] Rajesh B. R. D. Yamajala [b] and Adline Princy Solomon *[a]

Vibrio cholerae, the causative agent of cholera, poses a continuous threat to global public health, especially in regions with poor sanitation. Its ability to form biofilms and rapidly acquire antimicrobial resistance (AMR) complicates therapeutic interventions. In this study, the quorum-sensing (QS) response regulator LuxO was targeted for anti-virulence therapy using a synthesized pyridine-based compound, QSI^{py}. Pyridine derivatives are explored as inhibitors that can target the LuxO protein, a key regulator in the QS pathway of *V. cholerae*. By inhibiting LuxO, these compounds reduced the virulence factor expression and biofilm formation, offering a novel antivirulence strategy without promoting resistance. Molecular docking showed that QSI^{py} exhibited a strong binding affinity, with a glide score of −5.046 at the ATP-binding domain of LuxO. *In vitro* evaluation revealed that QSI^{py} had no inhibitory effect on planktonic bacterial growth, indicating a non-bactericidal mechanism. However, it showed significant inhibition of biofilm formation, as confirmed by crystal violet assay and quantified through MBIC determination. Pellicle CFU enumeration demonstrated a reduction in viable biofilm-associated cells, particularly at the lowest concentrations of 15.6 μg mL^{-1} and 31.2 μg mL^{-1}, while fluorescence microscopy validated the loss of pellicle integrity. Additionally, checkerboard synergy testing with azithromycin (AZM) revealed a high synergy score based on Bliss independence modelling, whereas no synergy was observed with ciprofloxacin or doxycycline. These results suggest that QSI^{py} potentiates macrolide antibiotic activity by interfering with quorum-sensing-regulated biofilm and virulence expression.

Received 7th August 2025
Accepted 21st January 2026

DOI: 10.1039/d5ra05777a

rsc.li/rsc-advances

Introduction

Vibrio cholerae is a curved, rod-shaped, Gram-negative bacterium that inhabits the small intestine and secretes cholera toxin (CT), resulting in profuse fluid secretion and dehydration. The bacterium consists of a single polar flagellum, which facilitates motility; it is also facultatively anaerobic and oxidase-positive and can survive under diverse environmental conditions such as brackish waters, estuaries, and marine coastal ecosystems.[1] The symptoms of cholera vary from mild diarrhea to profuse watery stools, referred to as "rice-water" stools. Cholera can lead to heavy loss of electrolytes and dehydration if left untreated. According to the World Health Organization (WHO), the condition remains a serious public health issue worldwide, especially where there is poor sanitation and limited clean water availability. Based on the presence of the O antigen of lipopolysaccharide, *V. cholerae* can be categorized into more than 200 serogroups. Serogroup O1 causes an epidemic that consists of two biotypes: classical and El Tor. The classical biotype caused the previous pandemics, while the El Tor biotype has prevailed since the seventh pandemic, which started in 1961 and continues to exist.[2] *V. cholerae* maintains a complex life cycle that shifts between aquatic reservoirs and human hosts. It can survive for prolonged periods under unfavourable conditions in the environment in a viable but non-culturable (VBNC) condition. The pathogen enters the small intestine through food or water, moves within the acidic environment, and colonizes in the jejunum and ileum.[3] Toxin-coregulated pilus (TCP) is one of the surface features that facilitates colonization and is crucial for microcolony establishment and intestinal adhesion.[4] TCP has dual functions: it acts as an intermediate in adhesion to the intestinal epithelium and acts as a receptor for the lysogenic bacteriophage CTXΦ, which contains the ctxAB genes encoding for CT.[4,5] CT is the major toxin that leads to watery diarrhea. CT is an AB5 exotoxin with one enzymatically active A subunit (CtxA) and five binding B subunits (CtxB). The B subunits attach to the GM1 ganglioside receptors on the intestinal epithelial cell surfaces, enabling endocytosis and retrograde transport of the A subunit into the cytosol.[6] Upon cellular entry, CtxA catalyzes the ADP-ribosylation of the Gsα protein and causes constitutive activation of adenylate cyclase. Elevated levels of cyclic AMP (cAMP) follow, which stimulate the cystic fibrosis transmembrane conductance regulator (CFTR) chloride

[a]*Quorum Sensing Laboratory, Centre for Research in Infectious Diseases (CRID), School of Chemical and Biotechnology, SASTRA Deemed to Be University, Thanjavur, India. E-mail: adlineprinzy@sastra.ac.in*

[b]*Organic Synthesis & Catalysis Laboratory, School of Chemical and Biotechnology, SASTRA Deemed to Be University, Thanjavur, India*

channels to cause efflux of chloride ions and water into the lumen of the intestine.[7] LuxO is a central response regulator in the *V. cholerae* QS system, a mechanism that allows bacteria to sense group behavior as a function of population density.[8] Under low cell density, LuxO is phosphorylated by upstream sensor kinases. The phosphorylated LuxO induces small regulatory RNAs expression (Qrr sRNAs) through σ^{54}, which then represses HapR translation, which is the master QS regulator. Suppression of HapR at low cell density enables the expression of virulence genes, such as cholera toxin (ctxAB) and toxin-coregulated pilus (tcpA), which facilitate colonization and infection.[9] Dephosphorylation of LuxO at high cell density results in enhanced HapR expression, which represses virulence and biofilm genes and induces bacterial dispersal. Being a molecular switch in virulence regulation, LuxO is also a target with high promise for anti-virulence therapy that will incapacitate *V. cholerae* without inducing antimicrobial resistance.[10] Apart from CT and TCP, *V. cholerae* also produces various accessory virulence factors that are involved in colonization, epithelial damage, and inflammation. In *V. cholerae*, antibiotic resistance to drugs such as tetracycline, ampicillin, and ciprofloxacin has been documented worldwide.[11] AMR in cholera strains represents a critical challenge for the treatment of the disease, particularly in epidemics, as it restricts the effective use of antibiotics and increases the potential for complications and transmission. The administration of ineffective drugs can aggravate the clinical course by postponing therapy with the correct drug, prolonging the duration and intensity of diarrhoea, and extending bacterial excretion, which enhances transmission risk in epidemic situations.

Pyridine and its derivatives are aromatic nitrogen-heterocyclic compounds with a wide range of antimicrobial properties. Many pyridine-based molecules have been synthesised recently to screen their extensive activity against various pathogens, including *Vibrio cholerae*. Pyridine derivatives can inhibit DNA gyrase, quorum-sensing circuit, and break down the bacterial membrane integrity. Several studies have shown that pyridines with substituted groups reduce the production of cholera toxin and disrupt biofilm formation, which is crucial for bacterial colonisation and persistence within the host. For instance, pyridine derivatives that are halogenated and alkylated have exhibited strong *in vitro* inhibitory activity against *V. cholerae* strains by disrupting the bacterial cell wall and interfering with regulatory proteins used in toxin expression. These results imply that pyridine scaffolds can be engineered into new antimicrobial agents that hold the potential to break existing resistance. Due to their structural flexibility and pharmacological promise, pyridine derivatives are being pursued intensively as lead compounds for novel anti-cholera drugs, and specifically against multidrug-resistant strains of *V. cholerae*.[12]

To combat increasing antimicrobial resistance in *V. cholerae*, our research evaluates a new anti-virulence approach against the LuxO regulator by using pyridine-derived quorum-sensing inhibitors. On the back of evidence that such compounds, including pyrazine derivatives, inhibit biofilm development, virulence gene expression, and act synergistically with antibiotics by inducing high-cell-density responses prematurely,[13] we plan to screen lead pyridine molecules through *in silico* screening and docking, synthesise the best candidate, and assess its anti-biofilm and antimicrobial activity *in vitro*. The purpose of this study is to evaluate its possible synergy with traditional antibiotics, hoping to provide a resistance-free therapeutic pathway for treating *V. cholerae* infections.

Results and discussion

Homology modelling

Using BLASTp, the amino acid sequence of LuxO protein from *V. cholerae* (Q9KT84) was compared with other known protein structures, as previously reported.[14] The LuxO receiver-catalytic domain from *Photobacterium angustum* (5EP0_A) had 78.54% sequence similarity with a 1.6 Å resolution X-ray structure and was used as a template for homology modelling of the LuxO protein (Fig. 1). The topology of the modelled protein is like the response regulator fold, which suggests that both the receiver and the catalytic domain are successfully modelled. The central core of the modelled protein is surrounded by the helices, which implies stability and integrity of the protein. This model serves as the basis of validation for further docking analysis. The modelled *V. cholerae* LuxO protein structure was evaluated using the Ramachandran plot (Fig. 2). The plot shows that the majority of the amino acid residues fall within the favoured (red) and allowed (yellow) regions, which indicates the protein has a well-modelled protein backbone conformation. Few amino acid residues, for example, Asp248, fall in disallowed regions, which suggests that the protein is structurally reliable for further analysis, and they do not significantly affect the overall structural quality of the modelled protein. The high percentage of amino acid residues lying in the favoured region validates the modelled protein's conformational quality. The modelled protein was furthermore validated using the ProCheck and Errat tools (Fig. 3). Most of the residues have scores above 95% confidence threshold, suggesting this modelled protein is a reliable model. Few regions around the residues

Fig. 1 Three-dimensional homology model of the LuxO protein from *V. cholerae* generated using SWISS-MODEL with 5EP0_A as a template from *Photobacterium angustum*.

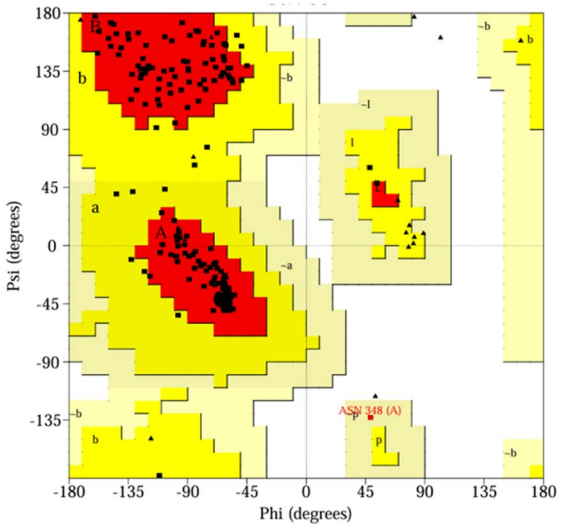

Fig. 2 Structure validation of the homology-modelled LuxO protein by a Ramachandran plot using PROCHECK.

260–270 (marked in red) cross the 99% confidence threshold. This suggests that these residues are either flexible or poorly modelled, but the overall model quality is not compromised as they are unlikely to impact ligand binding or other predictions.

Molecular docking

All the 50 compounds identified as pyridine derivatives were docked with the active sites of the LuxO modelled protein. Compound **3**-((3-fluoro-4-(piperidin-1-yl)phenyl)carbamoyl) picolinic acid (QSI^{py}) demonstrated the highest Glide score of -5.046 kcal mol^{-1} with LuxO protein, followed by 5-bromo-3-((3-fluoro-4-(piperidin-1-yl)phenyl)carbamoyl)picolinic acid (Fig. 4). The 2D interaction (Fig. 5) provides insights into the binding interactions of the ligands within the LuxO protein. It shows the involvement of amino acids Lys166, Glu167 and Asp231 in the stabilisation of the ligand in the binding pocket of the LuxO protein by forming hydrogen bonds. Other stabilising forces, such as van der Waals interactions and hydrophobic contacts, are also present. There are possible electrostatic interactions that complement the shape and stability, suggesting that the ligand is suitably aligned in the catalytic site and is not tightly bound. The 3D representation of the docked ligand (Fig. 6) shows the ligand within the modelled LuxO protein, where it occupies the defined cavity in the catalytic domain. This proper orientation of the ligand ensures optimal interactions with the surrounding amino acid residues, enforcing proper structural stability. This also validates the ligand–protein interactions observed in 2D. The arrangement of the ligand is such that it is surrounded by α-helices, a hallmark of regulatory proteins. The positioning of the ligand allows favourable interaction within the catalytic domain with surrounding amino acid residues, which validates the docking results. This supports the hypothesis that the compound could act as an LuxO inhibitor, which interrupts the quorum sensing and signalling pathways in *V. cholerae.*

Synthesis of 3-((3-fluoro-4-(piperidin-1-yl)phenyl)carbamoyl) picolinic acid (QSI^{py})

The compound **3**-((3-fluoro-4-(piperidin-1-yl)phenyl)carbamoyl) picolinic acid (**5**), termed as QSI^{py}, was synthesized in three steps involving the general synthetic route[13] shown in Fig. 7. The synthesis was initiated by the aromatic nucleophilic substitution reaction of 3,4-difluoronitrobenzene and piperidine, in the presence of diisopropylethylamine, in acetonitrile at room temperature to afford the intermediate compound, 1-(2-fluoro-4-nitrophenyl)piperidine. Subsequent reduction with Fe/NH_4Cl in a methanol–water mixture yielded 3-fluoro-4-(piperidin-1-yl)aniline. Final amidation reaction with pyridine-2,3-dicarboxylic anhydride afforded the target compound QSI^{py} in good yield (85%).

3-((3-Fluoro-4-(piperidin-1-yl)phenyl)carbamoyl)picolinic acid (5)

Grey solid. Yield: 85%. ^{1}H NMR (600 MHz, DMSO-d_6) δ 10.59 (br s, 1H), 8.77 (dd, J = 2.28 Hz, 1.38 Hz, 1H), 8.18 (dd, J = 7.86 Hz,1.44 Hz, 1H), 7.68 (m, 2H), 7.44 (dd,J = 8.64 Hz, 2.40 Hz, 1H), 7.03 (t,J = 9.3 Hz, 1H), 2.93 (m, 4H), 1.66 (m, 4H), 1.53 (m, 2H). ^{13}C NMR (150 MHz, $CDCl_3$) δ 165.27, 163.67, 156.06, 154.42, 149.84, 145.52, 143.65, 139.28 (J_{C-F} = 8.7 Hz), 130.46 (J_{C-}

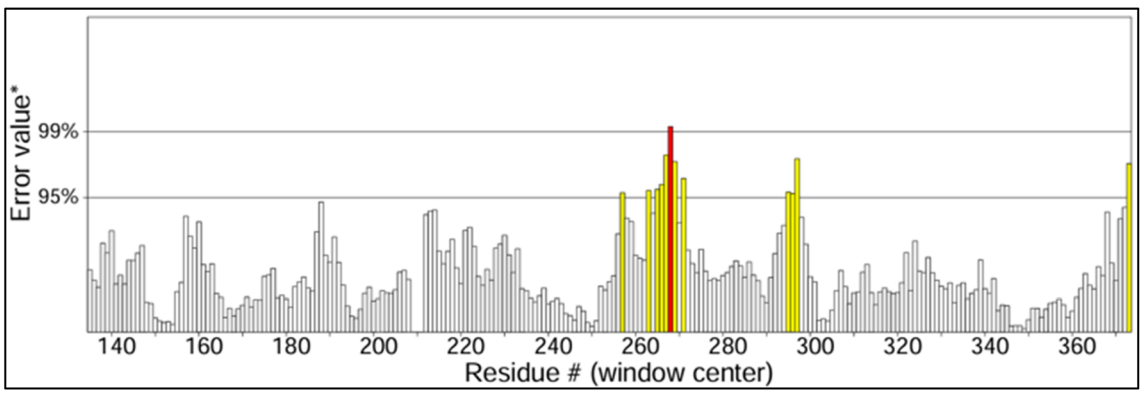

Fig. 3 ERRAT quality–factor plot evaluating the overall reliability of the homology-modelled LuxO protein.

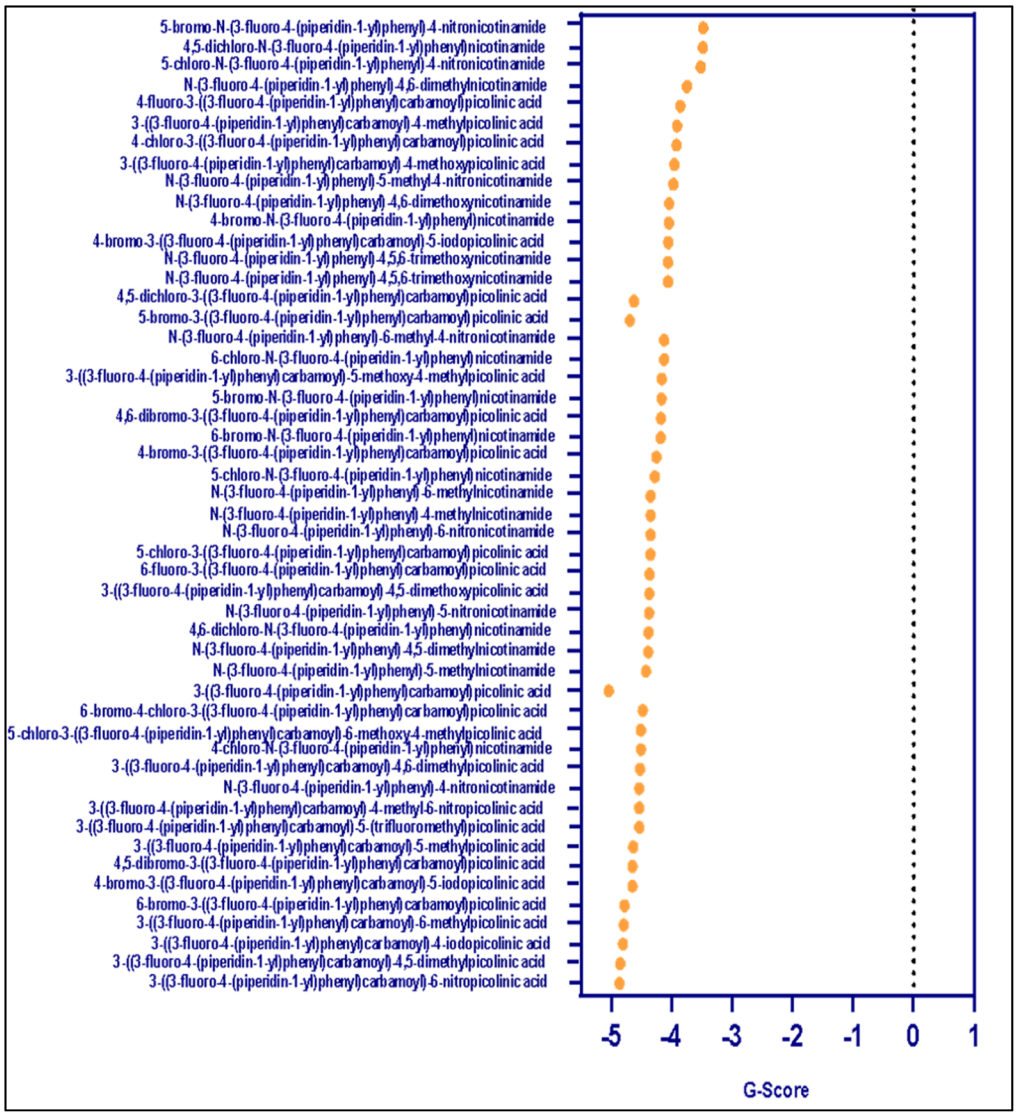

Fig. 4 Glide docking scores of pyridine-based derivatives screened against the modelled LuxO protein.

$_F$ = 56.7 Hz), 127.21, 119.07 (J_{C-F} = 69 Hz), 109.53 (J_{C-F} = 25.6 Hz), 52.04 (J_{C-F} = 63 Hz), 29.65, 26.00, 24.07. HRMS *m*/*z* calculated for $C_{18}H_{18}FN_3O_3$ = 344.1405 ($[M + H]^+$); found = 344.1411.

Minimum inhibitory concentration

The minimum inhibitory concentration (MIC) assays were conducted to assess the bacteriostatic or bactericidal activity of the synthesized compound QSI^{py} against *V. cholerae* strains HYR14 and MTCC3906. QSI^{py} was screened in a range of concentrations from 0.48 to 125 μg mL^{-1} by the broth microdilution technique in a 96-well plate format. The growth of bacteria was observed through measurement of optical density at 595 nm after 18–24 hours of incubation at 37 °C. The findings revealed that QSI^{py} did not have any appreciable inhibition of planktonic growth for either strain at any of the concentrations tested. In Fig. 8, both strains showed comparable growth patterns in the absence (negative control) and presence of the compound, suggesting that QSI^{py} has no direct antibacterial activities under planktonic conditions. The positive control (PC) shows a drastic reduction in growth, confirming that the assay can detect strong growth inhibition. The absence of MIC activity implies that QSI^{py} is not targeting the critical bacterial survival pathways, but rather potentially through non-lethal factors such as quorum-sensing interference or disruption of the biofilm. This observation warranted further assessment of QSI^{py} for anti-biofilm activity using MBIC and CFU-based assays.

Minimum biofilm inhibitory concentration

To determine the biofilm–inhibitory activity of QSI^{py}, minimum biofilm inhibitory concentration (MBIC) assays were performed using the crystal violet staining technique. Both *V. cholerae* strains, HYR14 and MTCC3906, were treated with serial concentrations of QSI^{py} from 0.48 μg mL^{-1} to 31.57 μg mL^{-1} in 96-well plates under static conditions for 24 hours. EDTA served as the positive control, which can be used as a standard anti-biofilm as well as an antibacterial agent for Gram-negative

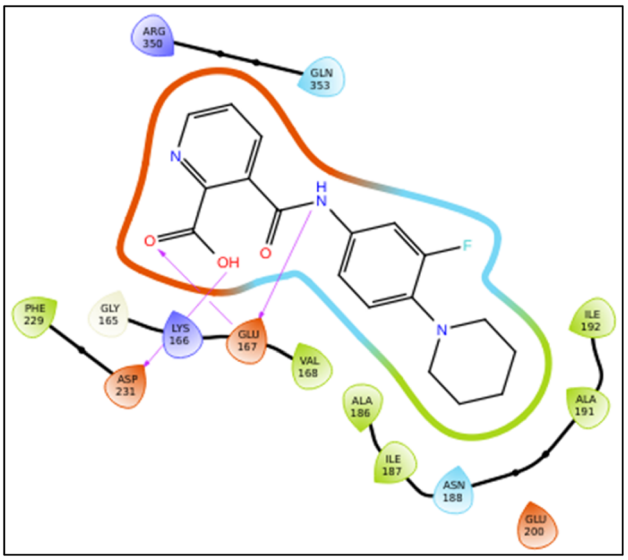

Fig. 5 Two-dimensional representation of the docked complex of QSI^{py} with LuxO from *Vibrio cholerae*, showing hydrogen-bond interactions with amino acid residues K166, E167, and D231.

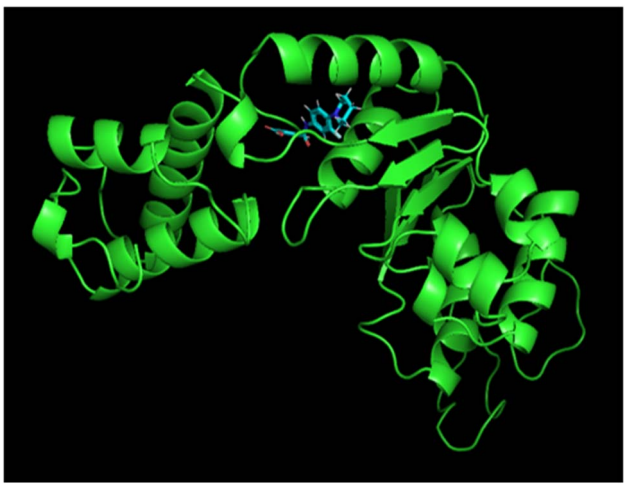

Fig. 6 Three-dimensional image of the docked complex of QSI^{py} (cyan stick) bound to LuxO from *Vibrio cholerae* (green cartoon), illustrating hydrogen-bond interaction within the ATP binding site.

bacteria, including *Vibrio cholerae*.[15] Biofilm biomass was stained with crystal violet post-incubation and read at 595 nm after solubilising the stain with acetic acid. QSI^{py} showed anti-biofilm activity in both strains. Notably, there was a substantial reduction in biofilm at lower concentrations, which continued down to 0.48 μg mL^{-1} (Fig. 9). In HYR14, QSI^{py} resulted in approximately 40–50% biofilm biomass reduction at 1.95 μg mL^{-1}. In MTCC3906, the compound showed even higher sensitivity, and inhibition was notable at lower concentrations of 3.9 μg mL^{-1}. This difference could be due to strain-specific reaction or variation in biofilm structure. These findings strongly indicate that QSI^{py} disrupts biofilm formation processes without blocking bacterial growth, most probably by inhibiting quorum sensing or signaling pathways that regulate biofilm maturation. The MBIC results concur with *in silico* predictions against LuxO, a key regulator of quorum sensing and virulence in *V. cholerae*. The strong inhibition of biofilm at sub-MIC concentrations indicates the therapeutic promise of QSI^{py} as a non-bactericidal anti-virulence compound, especially for chronic and resistant cholera infections. The low $MBIC_{50}$ values suggest that both compounds are potent biofilm inhibitors, particularly HYR14, which showed stronger inhibition at lower concentrations. These findings indicate that QSI^{py} functions as a non-bactericidal anti-virulence factor, likely inhibiting quorum-sensing processes—consistent with its predicted binding to LuxO. Its high activity at sub-MIC concentrations underscores its value for the treatment of chronic cholera infections.

Enumeration of colony forming units from biofilm pellicles

Cells in biofilms and pellicles exhibit strong resistance to several antibiotics compared to planktonic cells.[16] To assess the anti-biofilm potential of the pyridine compound QSI^{py}, viable cell counts were determined from pellicle biofilms of *V. cholerae* strains HYR14 and MTCC3906 after treatment with varying concentrations of the compound (3.9–125 μg mL^{-1}) (Fig. 10). In both strains, treatment with QSI^{py} resulted in a concentration-dependent reduction in CFU counts compared to the untreated control. EDTA served as the positive control, which can be used as a standard antibiofilm as well as an antibacterial agent for Gram-negative bacteria, including *Vibrio cholerae*.[15] For QSI^{py}_HYR14, a significant decrease in viable cell count was observed at 125 μg mL^{-1}, and the reduction persisted at all concentrations down to 3.9 μg mL^{-1}. Similarly, QSI^{py}_MTCC3906 displayed a marked reduction in CFU at 125 and 62.5 μg mL^{-1}, with significant inhibitory effects maintained even at 3.9 μg mL^{-1}. The observed reduction in CFU counts from biofilm pellicles indicates that the pyridine compound QSI^{py} effectively impairs the viability of *V. cholerae* biofilm-associated cells. Both clinical HYR14 and reference MTCC3906 strains exhibited significant susceptibility to QSI^{py}, even at low concentrations. Notably, the compound showed stronger inhibitory effects against the MTCC3906 strain at higher concentrations, suggesting possible strain-specific sensitivity. These results suggest that QSI^{py} may interfere with biofilm integrity or cell survival mechanisms within the pellicle matrix. The dose-dependent decrease in CFU counts supports its potential as a promising anti-biofilm agent. This also aligns with prior *in silico* findings targeting quorum-sensing pathways, particularly the LuxO regulator. The consistent decrease in viable biofilm cells further reinforces the potential of pyridine-based molecules in disrupting biofilm-associated persistence and resistance in *V. cholerae*. The observed decrease in viable cell numbers for all concentrations demonstrates that QSI^{py} interferes with the survival of *V. cholerae* HYR14 in the matrix of the biofilm. The dose-dependent trend implies that the compound can interfere with important processes in maintaining the biofilm, possibly by inhibiting quorum-sensing. Even though it does not eliminate cells, QSI^{py} drastically

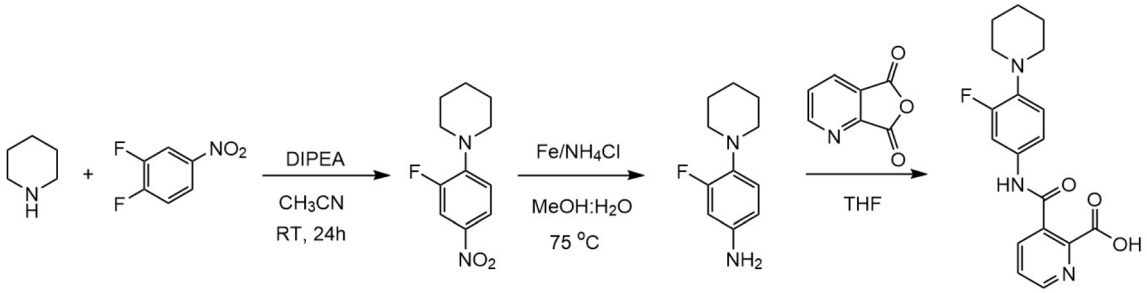

Fig. 7 Schematic route for the synthesis of the compound 3-((3-fluoro-4-(piperidin-1-yl)phenyl)carbamoyl)picolinic acid (QSI^{py}). The reaction of piperidine and 1,2-difluro-4-nitrobenzene using DIPEA in acetonitrile at room temperature for 24 h, followed by reduction of the nitro intermediate to the amine with iron and ammonium chloride in methanol–water at 75 °C. The resulting amine substrate is then coupled with picolinic acid in tetrahydrofuran (THF).

decreases CFU even at lower concentrations, validating its position as a strong anti-biofilm compound. These results are consistent with earlier *in silico* predictions of LuxO-targeted quorum-sensing inhibition, underlining the therapeutic promise of QSI^{py} in counteracting biofilm-mediated resistance to cholera infection.

Fluorescence imaging

The qualitative findings supported the quantitative data obtained from viable cell count analysis of the biofilm pellicles. A significant reduction in the number of pellicle cells is observed in Fig. 11 through the fluorescence imaging of the compound across varying concentrations from 31.2 μg mL^{-1} to 7.9 μg mL^{-1}. A dense network of biofilms was seen in the control, and individual pellicle cells could be seen in the treatment groups. The green colour indicates the presence of live cells in the bacterial pellicle load. The analysis demonstrated that QSI^{py} effectively disrupts pellicle biofilm formation in both *V. cholerae* strains HYR14 and MTCC3906 in a concentration-dependent manner. The control samples showed dense green fluorescence, indicative of intact and viable pellicle biofilm structures. EDTA served as the positive control, showing strong biofilm inhibition. Treatment with QSI^{py} led to a visible reduction in fluorescence intensity and pellicle cell density, with minimal

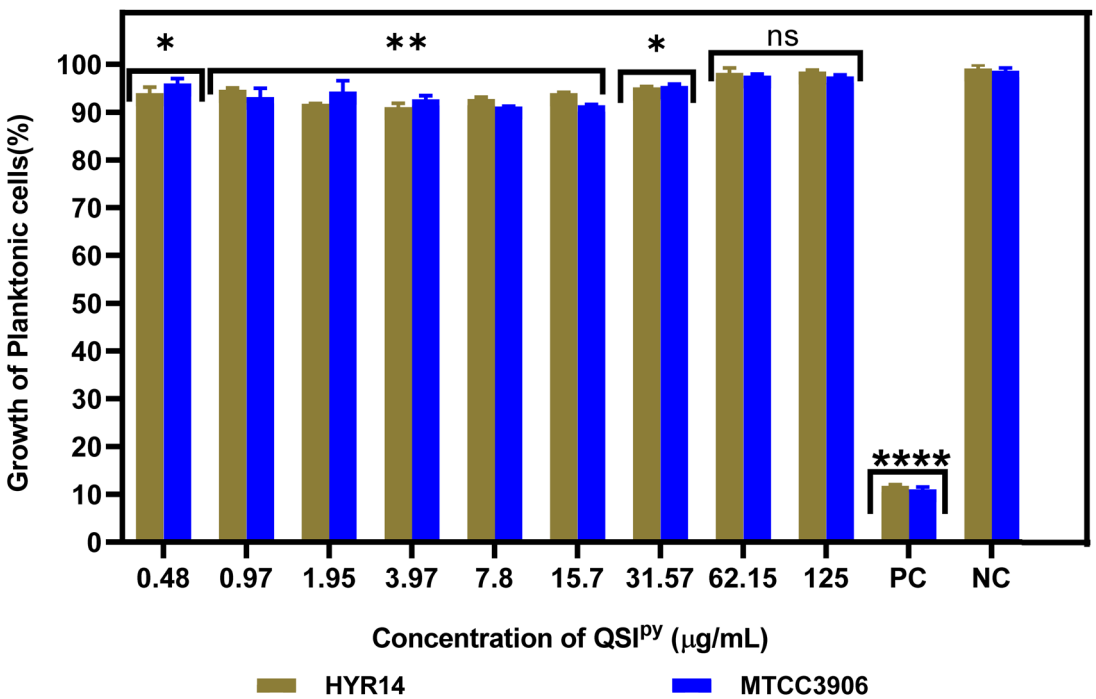

Fig. 8 Effect of QSI^{py} on the planktonic growth of HYR14 and MTCC3906. Growth of the planktonic cells (%) of HYR14 (brown bars) and MTCC3906 (blue bars), following treatment with increasing concentrations of QSI^{py} (0.49–125 μg mL^{-1}). Within the concentrations of 0.49–125 μg mL^{-1}, both HYR14 and MTCC3906 maintain planktonic growth similar to the untreated negative control (NC). The positive control (PC) shows a drastic reduction in growth, confirming that the assay can detect strong growth inhibition. Statistical significance between treated groups and NC is indicated as *$p < 0.05$, **$p < 0.01$, ****$p < 0.0001$; ns, not significant; $n = 3$.

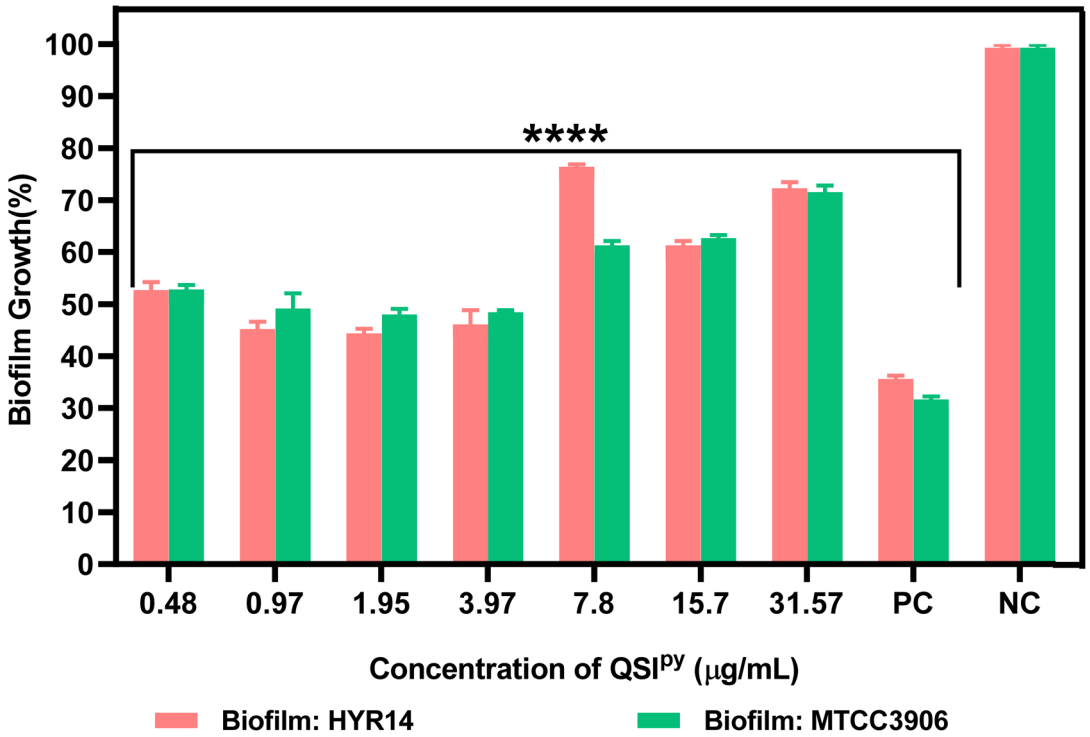

Fig. 9 Inhibition of biofilm formation by QSI^{py} against HYR14 and MTCC3906. Biofilm growth (%) of HYR14 (pink bars) and MTCC3906 (green bars), following treatment with increasing concentrations of QSI^{py} (0.48–31.57 μg mL^{-1}). Data are expressed as mean ± SD of three independent experiments ($n = 3$). The positive control (PC) shows minimal biofilm growth, while the negative control (NC) represents untreated cells with no inhibition. Statistical significance across QSI^{py}-treated groups is indicated as ****$p < 0.0001$.

signal observed at 15.6 μg mL^{-1} and 31.2 μg mL^{-1}. This suggests a significant loss of biofilm-associated cells. Notably, MTCC3906 exhibited greater sensitivity at lower concentrations, aligning with the CFU reduction data. These findings reinforce the anti-biofilm efficacy of QSI^{py} and support its potential as a quorum-sensing-targeted therapeutic agent. These qualitative observations are also consistent with the CFU data and again show the strong biofilm-disrupting activity of QSI^{py}. The declining green fluorescence in proportion to increasing concentrations evidences compromised viability and structural cohesion of the biofilm pellicles. Strikingly, strain MTCC3906 was more sensitive in lower concentrations and showed a considerable reduction, even at 7.9 μg mL^{-1}. This confirms the postulate that QSI^{py} inhibits quorum sensing or biofilm maintenance mechanisms. Collectively, the microscopic findings corroborate the efficacy of QSI^{py} as an anti-biofilm agent against biofilm-residing cells of *V. cholerae*.

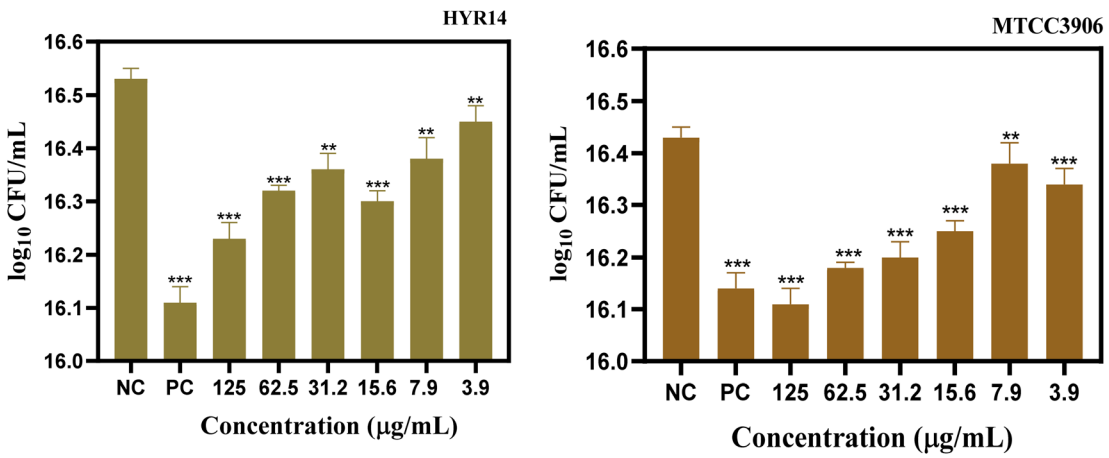

Fig. 10 Enumeration of colony-forming units from the pellicle biofilms of HYR14 and MTCC3906 strains of *V. cholera* post treatment with QSI^{py} at varying concentrations compared with the negative control (NC). The positive control (PC) represents lesser number of colonies. ($n = 3$, **$p <$ 0.01, ***$p < 0.001$).

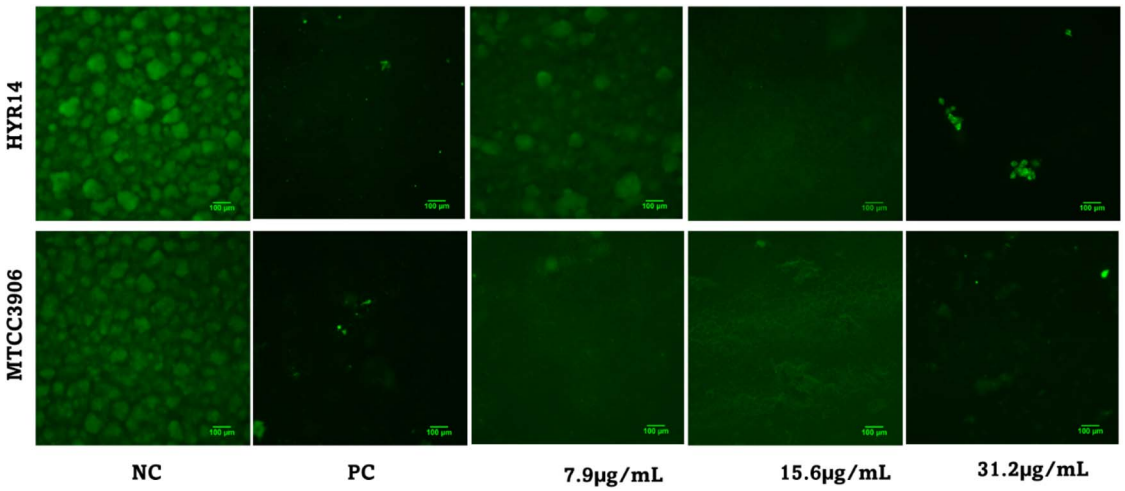

Fig. 11 Visualization of the biofilm pellicle of HYR14 and MTCC3906 strains of *V. cholerae* stained with SYTO9, depicting live cells in green under fluorescence microscopy when treated with QSI^{py} at varying pellicle biofilm inhibitory concentrations (PC = positive control, NC = negative control).

Checkerboard assay

The synergistic interaction of azithromycin (AZM) when combined with QSI^{py} was determined using the checkerboard assay, and the interaction was assessed with the Bliss independence model. The assay was conducted for differing concentrations of QSI^{py} (3.9 μg mL^{-1} to 0.1 μg mL^{-1}) in combination with AZM (25 μg mL^{-1} to 0.38 μg mL^{-1}). From Fig. 12, there was an evident synergistic interaction at low concentrations of both drugs. In particular, for strain HYR14, a synergy score of 31.04 was observed when AZM was administered at 1.5 μg mL^{-1} in combination with QSI^{py} at 3.98 μg mL^{-1}. Likewise, the MTCC3906 strain showed a synergy score of 45.81 at AZM 3.12 μg mL^{-1} and QSI^{py} 3.98 μg mL^{-1}. These observations show that QSI^{py} increases the activity of AZM over the activity of the drug alone in both strains. Conversely, no synergistic interaction was observed between QSI^{py} with doxycycline (DOX) or ciprofloxacin (CIP), as illustrated in Fig. S4(a and b), and the potentiating effect is likely to be specific to AZM. This is perhaps because AZM already inhibits protein synthesis and further has its quorum-sensing role disrupted by QSI^{py}. These findings establish the prospect of QSI^{py} as a quorum-sensing inhibitor that can enhance the efficacy of macrolide antibiotics such as AZM. These combinations may also decrease the amount of antibiotics needed, thus minimizing side effects and slowing down resistance emergence. In general, the findings affirm the therapeutic value of anti-quorum-sensing agents in combination with classical antibiotics for more efficient treatment of biofilm-associated and drug-tolerant *V. cholerae* infection. The co-treatment of QSI^{py} and AZM showed substantial synergistic inhibition of biofilms, notably in the case of MTCC3906. The activity enhancement implies that QSI^{py} enhances the anti-biofilm activity of AZM, potentially by disrupting quorum-sensing pathways that control biofilm stability and antibiotic tolerance. However, no significant synergy was seen with doxycycline or ciprofloxacin (data not shown), suggesting that potentiation by QSI^{py} is specific to macrolides such as AZM. This cooperative effect may enable decreased antibiotic dosing with preserved effectiveness, presenting a twofold benefit of reducing toxicity and retarding resistance emergence. In total, these findings establish the therapeutic potential of QSI^{py} as an adjuvant to standard antibiotics for the treatment of recalcitrant *V. cholerae* biofilms.

Minimum biofilm eradication concentration

The minimum biofilm eradication concentration (MBEC) of QSI^{py} against matured *V. cholerae* biofilms was quantitatively determined over a spectrum of concentrations (3.97–125 μg mL^{-1}). Fig. 13 displays the percentage of pre-formed biofilm growth in the standard reference strain MTCC3906 as well as the clinical isolate HYR14. A clear dose-dependent effect was noted in both strains. At 3.97 μg mL^{-1}, the lowest concentration studied, QSI^{py} induced a biofilm eradication of about 47.2% and 46.1% in HYR14 and MTCC3906, respectively. It can be inferred that sub-inhibitory levels of QSI^{py} are enough to weaken biofilm integrity considerably. Upon increasing the concentration to 7.8 μg mL^{-1}, eradication improved to 55.6% in HYR14 and 51.3% in MTCC3906, reflecting an improvement in anti-biofilm activity early on. Notably, at 15.7 μg mL^{-1}, the eradication efficacy reached a plateau to some extent, with HYR14 being 55.8% and MTCC3906 being 52.1%, indicating possible saturation of target quorum-sensing components in mid-range concentrations. However, by raising the concentration to 31.57 μg mL^{-1}, there was a sharp increase in the clearing of biofilms to 64.7% for HYR14 and 63.2% for MTCC3906. This suggests that this is a key threshold above which QSI^{py} has more effective biofilm disruption, potentially through complete repression of essential virulence and structural genes that maintain the biofilm. Maximum eradication was observed at 62.15 μg mL^{-1}, where MTCC3906 had a maximum of 69.3% of biofilm clearance, and HYR14 followed closely with 66.7%.

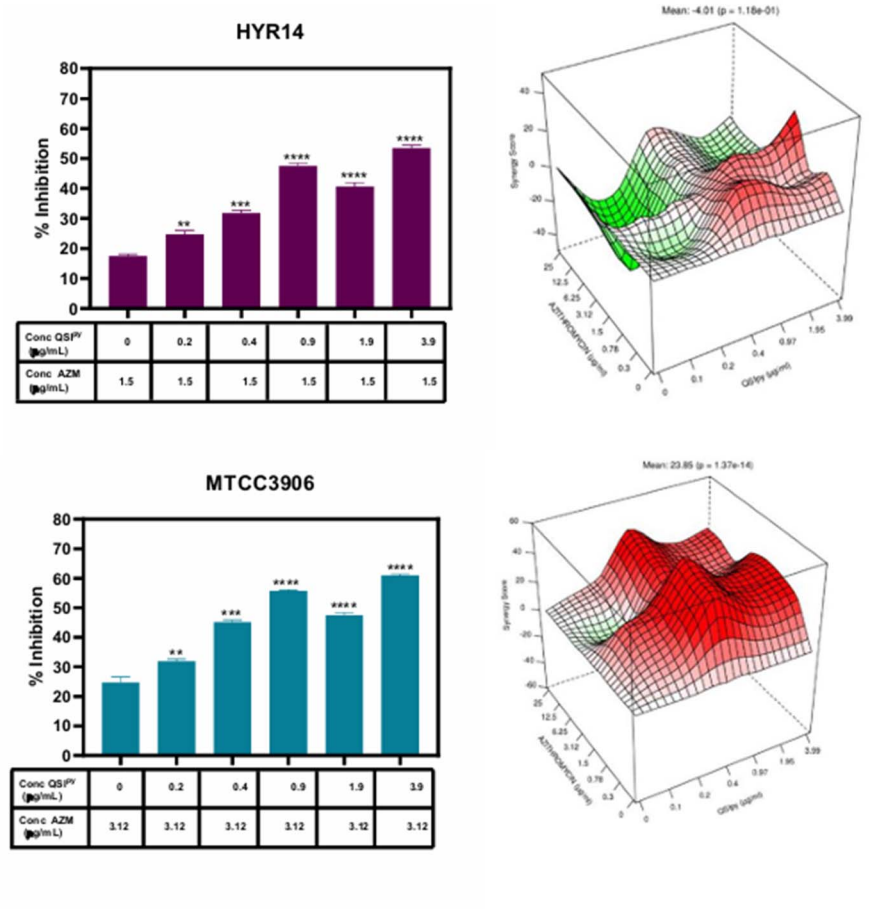

Fig. 12 Effect of QSI^{py} in enhancing the bactericidal activity of AZM. Synergy plot illustrating the combined effect of QSI^{py} and AZM at varying concentrations against HYR14 and MTCC3906. Potentiation of QSI^{py} was observed at a minimum concentration of 0.9 mg mL^{-1}, with AZM maintained at a constant concentration of 1.5 mg mL^{-1} and 3.12 mg mL^{-1} for HYR14 and MTCC3906, respectively. ($n = 3$, $^{**}p < 01$, $^{***}p < 0.001$, $^{****}p < 0.0001$ compared with the control).

These are strong anti-biofilm activities in fairly moderate concentrations of QSI^{py}. In general, MTCC3906 had marginally but consistently higher eradication rates compared to HYR14 at all concentrations, though differences were not statistically significant, pointing to QSI^{py} being as effective against both reference and clinical isolates. The graph of QSI^{py} reflects that it effectively inhibits biofilms in a concentration-dependent manner, specifically in the 31.57–62.15 μg mL^{-1} range. These findings closely match the downregulation of quorum-sensing and virulence genes found in qRT-PCR and infer that the biofilm disruption observed is mechanistically connected with the inhibition of important regulators such as *luxO*, *qrr4*, *aphA*, and virulence factors *ct* and *tcp*. Finally, the MBEC assay confirms that QSI^{py} has significant biofilm-clearing activity against *V. cholerae*, with optimal activity in the range of 31–62 μg mL^{-1}. This range might be a reasonable therapeutic target range for future preclinical or combination studies with QSI^{py} and other antimicrobial drugs. Crystal violet staining results (Fig. 14) visually confirmed the quantitative data. Untreated controls presented intense staining, suggesting the formation of dense biofilms. Conversely, biofilms treated with 7.9, 15.9, and 31.2 μg mL^{-1} of QSI^{py} demonstrated decreased staining intensity, which is in accordance with extensive biofilm disruption and detachment. Interestingly, both strains reacted in the same manner to QSI^{py} treatment, with MTCC3906 showing marginally greater eradication at higher concentrations. The uniformity of QSI^{py} action on both strains, particularly the clinical isolate HYR14, indicates its promise as a wide-spectrum quorum-sensing modulator with intense anti-biofilm activity. In combination, these observations suggest that QSI^{py} is capable of inhibiting mature *V. cholerae* biofilms at relatively low concentrations. The significant biofilm biomass loss, verified both quantitatively and qualitatively, suggests the potential utility of QSI^{py} in biofilm-associated infection control.

qRT-PCR profiling of gene expression

The impact of QSI^{py} on QS and virulence gene expression in *V. cholerae* was analyzed by qRT-PCR. The relative expression of several QS regulatory and virulence-associated genes, such as *luxO*, *qrr4*, *hapR*, *ct*, *tcp*, and *aphA*, was assessed in two strains, the reference strain MTCC3906 and the clinical isolate HYR14, before and after treatment with QSI^{py} at a concentration of 3.97 μg mL^{-1}. As demonstrated in Fig. 15a and b, QSI^{py} triggered

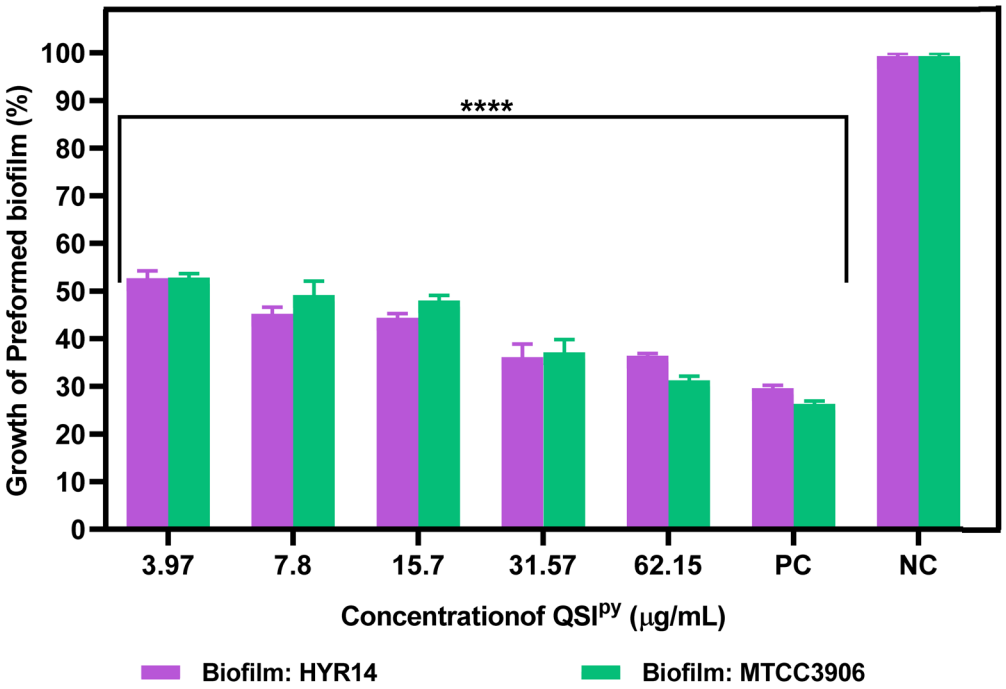

Fig. 13 Eradication of preformed biofilms by QSI^{py} against HYR14 and MTCC3906. Percentage of the growth of pre-established biofilm in HYR14 (purple bars) and MTCC3906 (green bars) following treatment with increasing concentrations of QSI^{py} (3.97–62.15 μg mL^{-1}). Data are presented as mean ± SD of three independent experiments ($n = 3$). The positive control (PC) represents minimal biofilm growth, while the negative control (NC) denotes untreated biofilms with no eradication. Statistical significance across QSI^{py}-treated groups is indicated as ****$p < 0.0001$.

specific transcriptional responses in both strains. The results showed that QSI^{py} substantially suppressed luxO and qrr4 expression in both strains (−3.50 and −1.37 $\log_2$ fold in MTCC3906; −3.94 and −2.64 in HYR14, respectively), demonstrating repression of the initial quorum-sensing cascade. This is consistent with the established role of QSI^{py} as a quorum-sensing modulator interacting with the autoinducer signaling network. Notably, hapR, the central QS transcriptional regulator active at high cell density (HCD), the master regulator of quorum sensing and virulence repression, was upregulated in both the strains following treatment (2.27 $\log_2$ fold in MTCC3906 and 1.68 in HYR14). This indicates that QSI^{py}-mediated repression of luxO has the indirect effect of liberating repression on hapR, supporting its expression and subsequent regulatory effects. Key among these was the downregulation of the virulence determinant genes *ct* (cholera toxin) and *tcp* (toxin co-regulated pilus) upon QSI^{py} treatment in both strains. In MTCC3906, ct and tcp decreased by −3.10 and −2.50 $\log_2$ fold, and in HYR14, by −3.35 and −2.15 $\log_2$ fold, respectively. The downregulation of primary virulence determinants identifies the anti-pathogenic activity of QSI^{py}. The virulence factor aphA, which is typically activated in low cell density and is critical for virulence gene expression, was also downregulated in both strains normally induced under conditions of LCD, was also

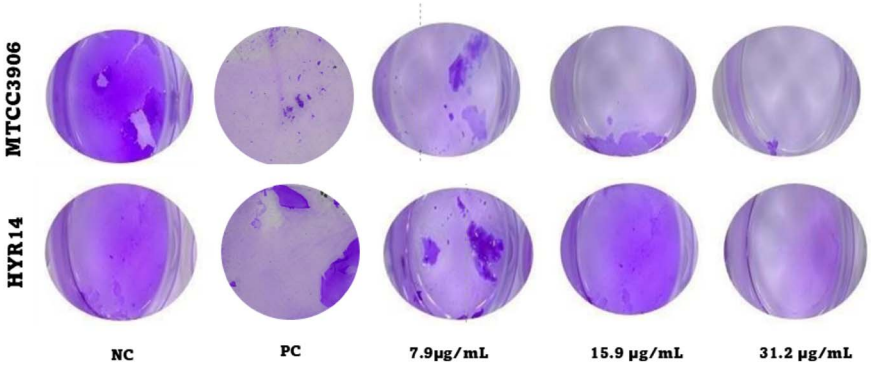

Fig. 14 Qualitative analysis of biofilm inhibition at varying concentrations of QSI^{py} performed using the crystal violet assay and visualized under a stereomicroscope. Treated cells showed a disturbed biofilm compared to the untreated control (NC = negative control, PC = positive control, $n = 3$).

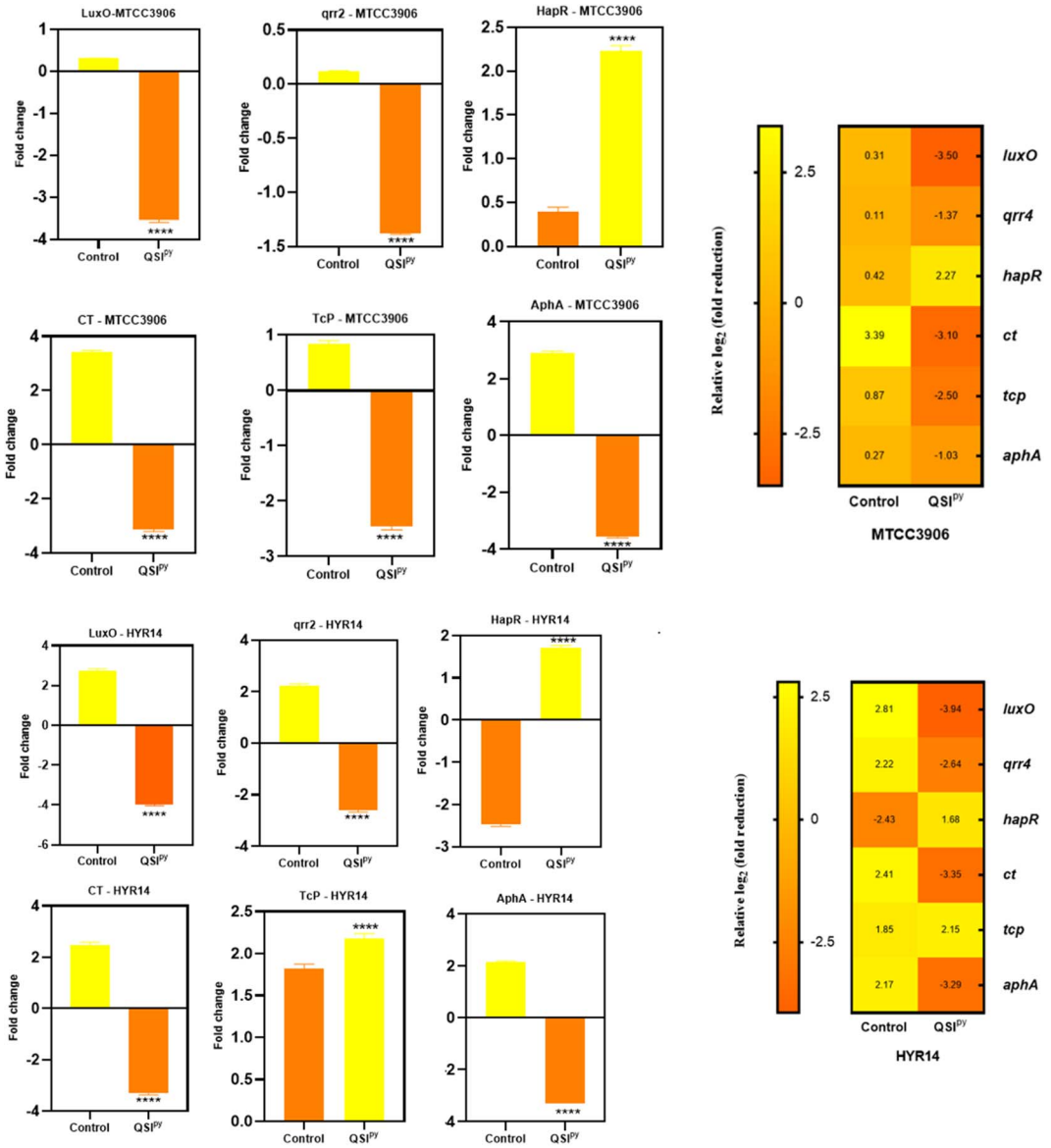

Fig. 15 (a) QSI^{py}-mediated modulation of quorum sensing and virulence gene expression in the MTCC3906 strains. The heatmap shows the relative $\log_2$ fold changes in key genes following the QSI^{py} treatment. Downregulation of *luxO, qrr4, ct, tcp,* and *aphA,* and upregulation of *hapR* indicate the disruption of quorum-sensing and virulence pathways. The bar graph represents the fold change of each gene compared with that of the control. ($n = 3$, ****$p < 0.0001$ compared with the control). (b) QSI^{py}-mediated modulation of quorum sensing and virulence gene expression in the HYR14 strains. The heatmap shows the relative $\log_2$ fold changes in key genes following the QSI^{py} treatment. Downregulation of *luxO, qrr4, ct, tcp, and aphA,* and upregulation of hapR indicate the disruption of quorum-sensing and virulence pathways. The bar graph represents the fold change of each gene compared with that of the control. ($n = 3$, ****$p < 0.0001$ compared with the control).

uniformly downregulated in both strains (−1.03 for MTCC3906 and −3.29 for HYR14), reflecting a departure from the state of virulence. Together, the outcomes reflect a strain-dependent but reproducible pattern of QS and virulence gene suppression after treatment with QSI^{py}. Interestingly, the clinical isolate HYR14 showed an increased level of gene suppression compared to the reference strain, indicating increased sensitivity. These observations are consistent with phenotypic observations and suggest the potential of QSI^{py} as a quorum-sensing inhibitor with anti-virulence activity against *V. cholerae.*

MTT cell viability assay

The cell-based MTT assay was used to investigate the toxic effect of the synthesised compound, QSI^{py}, on the HepG2 cell line. The yellow tetrazolium MTT (3-(4,5-dimethylthiazolyl-2)-2,5-diphenyltetrazolium bromide) is reduced in metabolically active cells as a part of the action of dehydrogenase enzymes, to generate reducing equivalents (NADH, NADPH). The results (Fig. 16) showed that the percentage viability of the HepG2 cell line was unaffected in the presence of the test compound at 10× and 100× concentrations compared to the untreated control cells.

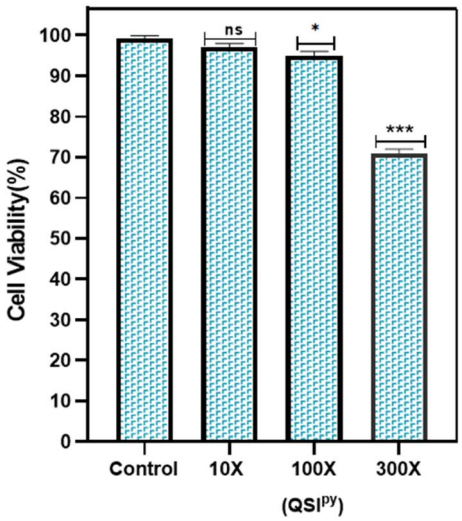

Fig. 16 Cell viability of the HepG2 cells treated with QSI^{py}. Cell viability (%), assessed after treatment at increasing QSI^{py} concentrations (10×, 100×, and 300×), showed no significant effect at 10× = 312 μg mL^{-1} compared with that of the control (ns, not significant). A significant reduction in cell viability was observed at 100× = 3120 μg mL^{-1} (*p < 0.05) and a highly significant decrease at 300× = 9360 μg mL^{-1} (***p < 0.001), indicating the dose-dependent cytotoxic response of the HepG2 cells upon QSI^{py} exposure.

Experimental methods

In silico evaluation

Template identification and sequence alignment. The FASTA sequence of the LuxO ATP-binding domain (Accession ID: Q9KT84) was retrieved from UniProt (https://www.uniport.org). The sequence was analysed through BLASTp against the Protein Data Bank to identify a structural template. The LuxO protein with the highest similarity, based on minimum *E*-value, sequence similarity, and availability of a solved crystal structure, was employed to model a homologous protein of LuxO. Pairwise alignment between the target sequence (Q9KT84) and the selected template (PDB ID: 5EP0_A) was carried out using ClustalW2 (https://www.ebi.ac.uk/Tools/msa/clustalw2/).

Homology modelling and structure validation. A three-dimensional model of LuxO was built based on the chosen template (5EP0) using the SWISS-MODEL server (https://swissmodel.expasy.org/). Following construction, energy minimisation of the modelled protein was executed in the SWISS-PDB viewer by adjusting bond length, angles, and other geometric distortions. Model reliability was assessed through PROCHECK (https://saves.mbi.ucla.edu/) using the Ramachandran plot to analyse stereochemical quality, and further validated with the ERAAT server to detect non-bonded interaction errors and evaluate the overall structural quality.

Molecular docking. The validated and modelled LuxO structure was then further processed with the help of the protein preparation Wizard in Schrödinger (Schrödinger, LLC, New York, NY, 2020) to eliminate water molecules, fix missing atoms, and alleviate steric clashes between amino acid residues. The protein structure was refined and energy-minimised to obtain an optimal conformation. A grid of receptors was generated around the ATP-binding domain of LuxO, and molecular docking was performed with the Extra Precision (XP) algorithm within the Glide module. The two-dimensional chemical structures of pyridine derivatives were discovered from PubChem and transformed into 3D structures with the LigPrep tool (Schrödinger, LLC, New York, NY, 2020). The docking was first done in Standard Precision (SP) mode, and then XP mode for the best-scoring ligands. The docking results were analysed based on Glide scores, important binding interactions, and functionality of groups interacting in the active site of the LuxO protein.

In vitro evaluation

Synthesis. The compound QSI^{py} was synthesised using appropriate reactions, and the structure was confirmed through NMR spectroscopy and HRMS (Fig. S1–S3).

Synthesis of 1-(2-fluoro-4-nitrophenyl)piperidine (3). To a stirred solution of piperidine **1** (11 mmol) in acetonitrile solution (15 mL), diisopropylethylamine (11 mmol) was added dropwise at 0 °C. 1,2-Difluoro-4-nitrobenzene **2** (11 mmol) was subsequently added to the above reaction mixture, and the reaction mixture was stirred overnight at room temperature. After completion, the mixture was poured into ice water, and the yellow precipitate obtained was filtered, washed with water, and dried in an open atmosphere to give compound **3**.

Synthesis of 3-fluoro-4-(piperidin-1-yl)aniline (4). To a stirred solution of compound **3** (5 mmol) in a methanol–water mixture (2 : 1, 18 mL), iron powder (30 mmol) and ammonium chloride (35 mmol) were added. The reaction mixture was refluxed for 5 hours, then cooled, and the resulting suspension was filtered through a Celite bed and washed with EtOAc (2 × 10 mL). The combined organic layers were dried over Na_2SO_4 and evaporated under reduced pressure to afford compound **4**.

Synthesis of 3-((3-fluoro-4-(piperidin-1-yl)phenyl)carbamoyl) picolinic acid (5). To a solution of 2,3-pyridinedicarboxylic anhydride (0.35 mmol) in THF (2 mL), compound **4** (0.35 mmol) was added and stirred at room temperature for 30 minutes, during which a precipitate formed. The solid was filtered, washed with petroleum ether, and dried under vacuum to obtain compound **5**, which was used in subsequent steps without chromatographic purification.

Bacterial strains and culture conditions. Strains of *V. cholerae* HYR14 and MTCC3906 were used throughout the study. To prepare the overnight culture, 5 μL aliquots of glycerol stocks were inoculated in 2 mL Luria Bertani (LB) broth and incubated at 37 °C for 18–24 hours. All culture media and reagents used were purchased from HiMedia, Mumbai. The overnight cultures were also streaked on LB agar plates and incubated under the same conditions; plates were kept at 4 °C for further use. LB broth was used as the standard culture medium for all the experimental work in this research.

Determination of minimum inhibitory concentration. The minimum inhibitory concentration (MIC) was found to assess the lowest concentrations of the test compounds that inhibit

visible growth of *V. cholerae*. Overnight cultures of fresh HYR14 and MTCC3906 strain colonies were grown in LB at 37 °C for 18–24 hours. Dimethyl sulfoxide (DMSO) was used to prepare the stock solution of the compound at a concentration of 30 μg mL^{-1}. Two-fold serial dilutions of 100 μL of QSI^{py} compound were prepared in LB in 96-well flat-bottom microplates. The concentrations ranged from 125 μg mL^{-1} to 0.48 μg mL^{-1}. The overnight bacterial culture was diluted to a ratio of 1 : 100 and employed to inoculate all wells. Thereafter, 10 μL of diluted bacterial suspension was inoculated into wells with serially diluted test compounds. EDTA at 266 μg mL^{-1} in 100 μM Tris buffer served as the positive control to validate the assay, based on the protocol reported by Adhikari *et al.* (1993).[17] Sterile media with bacterial culture was kept as a negative control to compare with the treated samples. The plate was incubated at 37 °C for 18–24 hours, after which absorbance was read at 595 nm using a microplate reader.[18]

Determination of minimum biofilm inhibitory concentration. The minimum biofilm inhibitory concentration (MBIC) was found to evaluate the anti-biofilm activity of QSI^{py} against *V. cholerae*. Overnight cultures of HYR14 and MTCC3906 were diluted according to the procedure detailed for the MIC determination and then added to a 96-well plate containing serial dilutions of QSI^{py} (125 μg mL^{-1} to 0.48 μg mL^{-1}). EDTA at 266 μg mL^{-1} in 100 μM Tris buffer served as the positive control to validate the assay, based on the protocol reported by Adhikari *et al.* (1993).[17] Sterile media with bacterial culture was kept as a negative control to compare with the treated samples. The optical density at OD_{595} of the planktonic cells was measured, and they were incubated at 37 °C for 24 hours. To remove planktonic cells, the plate was lightly tapped and then washed twice with PBS and air-dried for 5 to 10 minutes. 120 μL of 0.2% crystal violet was used to stain the cells for 15 minutes. The plate was air-dried after removing excess stain with water washes, and then the biofilm-bound stain was eluted using 150 μL of 33% acetic acid. The optical density was measured at 595 nm. The experiment was conducted in triplicate to ensure the accuracy and reproducibility of the results.[19–22]

Determination of colony forming units from biofilm pellicles. To quantify the viable bacterial cells within the pellicle, colony-forming unit (CFU) counts were performed. In brief, overnight cultures of HYR14 and MTCC3906 were diluted to 1 : 100 in fresh LB broth and inoculated into sterile glass tubes containing 3 mL of LB broth. The tubes were treated with QSI^{py} at varying concentrations from 125 μg mL^{-1} to 0.9 μg mL^{-1}, and the untreated tube served as a negative control. EDTA at 266 μg mL^{-1} in 100 μM Tris buffer served as the positive control to validate the assay, based on the protocol reported by Adhikari *et al.* (1993).[17] The plates were incubated statically for 48–72 hours without media replacement. After incubation, the pellicle formed at the air-liquid interface in the glass tubes was carefully removed using a sterile pipette tip. The pellicle was resuspended in 1 mL of sterile phosphate-buffered saline (PBS) by gentle pipetting. The suspension was serially diluted up to 10^{-12}, and 100 μL from each dilution was spread onto LB agar plates. The plates were then incubated at 37 °C for 24 hours for colony development, and colonies were counted. CFU mL^{-1} was calculated and used to compare bacterial load in treated and untreated samples.

Fluorescence microscopy. Fluorescence microscopy imaging was employed to visually investigate the pellicle inhibition potential of QSI^{py}. In a concise description of the method, the inoculum was cultured in a six-well plate with 3 mL of LB. Sterile coverslips were positioned, both in the presence and absence of the compound. The plate was treated with different biofilm inhibitory concentrations (ranging from 3.9 μg mL^{-1} to 0.9 μg mL^{-1}) of the compound. Untreated wells were retained as controls. EDTA at 266 μg mL^{-1} in 100 μM Tris buffer served as the positive control to validate the assay, based on the protocol reported by Adhikari *et al.* (1993).[17] After 24 h incubation at 37 °C, non-adherent planktonic cells were carefully removed, and the coverslips were gently washed twice with PBS. Utilising the Bac Light Bacterial Viability Kit (L7012), coverslips were stained as per the manufacturer's instructions using Syto9 dye, followed by a 10 min incubation in the dark. After eliminating excess stains and conducting two PBS washes, the coverslips were mounted onto glass slides. A Nikon Eclipse Ts2 microscope was used to capture fluorescence excitation images at a 10× magnification.[23]

Checkerboard assay. The potentiating effect of QSI^{py} against azithromycin (AZM), ciprofloxacin (CIP), and doxycycline (DOX) was measured by a checkerboard assay.[24,25] Briefly, two-fold serial dilutions of the compound QSI^{py} were performed in 96-well plates with 100 μL of LB broth from its biofilm inhibitory concentration of 3.9 μg mL^{-1} to 0.9 μg mL^{-1}. AZM, CIP, and DOX were added to wells at the same time, ranging from 8 μg mL^{-1} to 0.25 μg mL^{-1}. Individual concentrations of both compounds were also tested separately as controls. Overnight cultures of *V. cholerae* strains HYR14 and MTCC3906 were diluted to a ratio of 1 : 100 and inoculated into each well as per the MIC protocol. The well plates were incubated at 37 °C for 24 h, and the optical density was measured at 595 nm to determine the percentage of growth inhibition. SynergyFinder Plus was used to evaluate the data obtained using the Bliss independence model, which predicts the combined effect as the product of the individual effects, expressed by the formula $E_i = E_A \times E_B$ output.[19,26]

Determination of minimum biofilm eradication concentration. The biofilm eradication assay was conducted to find out the minimum dose of QSI^{py} capable of eliminating pre-formed biofilms of *V. cholerae*. Biofilms were grown in sterile 24-well microtiter plates. Overnight cultures of *V. cholerae* strains HYR14 and MTCC3906 were diluted 1 : 100 in fresh LB broth, and 100 μL of diluted suspension was added to the wells containing 1 mL of LB broth. The plates were statically incubated at 37 °C for 24 hours for biofilm development. After 24 hours of incubation, the planktonic cells were aspirated and gently washed twice with sterile phosphate-buffered saline (PBS) to eliminate non-adherent cells. Serial two-fold dilutions of QSI^{py} (125 μg mL^{-1} to 3.9 μg mL^{-1}) were made in LB broth. A relevant concentration of QSI^{py} was added to each well to treat the pre-formed biofilm and further incubated at 37 °C for 24 hours under static conditions. EDTA at 266 μg mL^{-1} in 100 μM Tris buffer served as the positive control. Sterile media with bacterial

culture was kept as a negative control to compare with the treated samples. After treatment, the wells were washed gently with distilled water twice to eliminate residual compounds and planktonic cells. Then, 0.2% of crystal violet was added to all the wells, which were then incubated for 15–20 minutes at room temperature. After the incubation, the surplus stain was removed by rinsing with distilled water and then eluted using 33% glacial acetic acid. The optical density was measured at 595 nm. The lowest concentration of QSI^{py} to inhibit visible growth after the recovery period was determined as the minimum biofilm eradication concentration. Crystal violet staining was employed to visualize the biofilm eradication of QSI^{py} against the *V. cholerae* strains. The same protocol was followed until the addition of 0.2% crystal violet stain, and it was rinsed twice with distilled water and allowed to air-dry. The biofilm eradication in the treated wells was visualized using stereomicroscopy (IVESTA3 Stereomicroscope).[27]

RNA extraction and qRT-PCR profiling of gene expression. Quantitative real-time PCR (qRT-PCR) was conducted to determine the expression change of *V. cholerae* genes following treatment with QSI^{py} at a concentration of 3.9 μg mL^{-1}. The cells were cultured under aerobic conditions for 24 hours at 37 °C in sterile tubes with and without the test compound. After incubation, planktonic cells were removed, and adherent bacterial cells were washed twice with sterile phosphate-buffered saline (PBS) and then harvested. The samples were centrifuged at 6000 rpm for 10 minutes, and the resulting supernatant was discarded. The pellet was used to extract the total RNA using the NucleoSpin®RNA kit as per the manufacturer's instructions. RNA concentration and purity were determined with a NanoDrop spectrophotometer (Thermo Scientific, USA). cDNA was prepared from isolated RNA by using a High-Capacity cDNA Reverse Transcription Kit (Applied Biosystems, Foster City, CA, USA), following the manufacturer's protocol, and was kept at −20 °C until used again. Gene expression was measured using SYBR Green-based qRT-PCR, with 16S rRNA as the housekeeping gene. Relative gene expression levels were determined by the 2^−ΔΔCT method.[28] Primers used in the study are listed in Table S1.

Cell viability assay. The cytotoxicity effect of QSI^{py} (10×, 100× and 300×) was tested on HepG2, which were obtained from the National Centre for Cell Science (NCCS), Pune, India, and the cell viability was measured using the MTT assay. HepG2 cells were maintained in Eagle's MEM supplemented with non-essential amino acids, 10% FBS and 1% Pen Strep. Briefly, the cells were resuspended to a density of 1×10^6 CFU mL^{-1} and 100 μL were seeded into 96-well plates, including a positive control (media and cells without the QSI^{py}) and a blank (media alone). Plates were incubated at 37 °C in 5% CO_2 until the cells reached confluence. The medium was then replaced with varying concentrations of test compound suspended in MEM medium and incubated for 24 h at 37 °C in 5% CO_2. After the incubation period, 20 μL of MTT solution (5 mg mL^{-1}) was added and incubated for 4 h. To this, 100% DMSO was added to each well, which were gently swirled for 10 min, and the absorbance was read at 570 nm. The percentage cell viability of QSI^{py}-treated HepG2 cells was calculated compared with the untreated cells.[14]

Statistical analysis. Statistical analysis was carried out with the help of GraphPad Prism software version 8.0.2 (GraphPad Software Inc., San Diego, CA, USA). The level of statistical significance was assessed using Student's *t*-test using a cutoff $p \leq 0.05$. The findings are presented as the average along with the standard deviation.

Conclusion

The current research identifies the quorum-sensing regulator LuxO as a viable target for anti-virulence interventions in *V. cholerae*. The pyridine derivative QSI^{py} was effective in binding with LuxO and greatly suppressed biofilm formation without suppressing bacterial growth. A combination of QSI^{py} with azithromycin also had synergistic effects, which improved its antimicrobial activity. These results suggest that QSI^{py} can be an effective anti-biofilm agent, compromising bacterial defenses and enhancing antibiotic efficacy, particularly against resistant *V. cholerae* strains. Hence, targeting the quorum-sensing regulator presents an effective and resistance-breaking therapeutic mechanism.

Author contributions

AS: Conceptualization, methodology, writing – original draft. DJA and VB: methodology, writing – original draft. APS: conceptualization, investigation, methodology, supervision, writing – review and editing. RBR: conceptualization, investigation, writing – review and editing.

Conflicts of interest

The authors declare that they have no conflicts of interest related to this work.

Data availability

The datasets generated and analyzed during the current study are available from the corresponding author upon reasonable request.

Supplementary information (SI): Fig. S1–S4 and Table S1. See DOI: https://doi.org/10.1039/d5ra05777a.

Acknowledgements

A. S., R. B. R. and A. P. S. sincerely thank the management of SASTRA Deemed University for providing the necessary facilities and support for this research. The authors would like to extend their thanks to all the scholars of the Quorum Sensing Lab (QSL).

References

1 R. R. Colwell, P. Brayton, D. Herrington, B. Tall, A. Huq and M. M. Levine, Viable but non-culturable Vibrio cholerae O1

revert to a cultivable state in the human intestine, *World J. Microbiol. Biotechnol.*, 1996, **12**(1), 28–31.
2 J. B. Kaper, J. G. Morris and M. M. Levine, Cholera, *Clin. Microbiol. Rev.*, 1995, **8**(1), 48–86.
3 E. J. Nelson, J. B. Harris, J. G. Morris, S. B. Calderwood and A. Camilli, Cholera transmission: the host, pathogen and bacteriophage dynamic, *Nat. Rev. Microbiol.*, 2009, **7**(10), 693–702.
4 D. A. Herrington, R. H. Hall, G. Losonsky, J. J. Mekalanos, R. K. Taylor and M. M. Levine, Toxin, toxin-coregulated pili, and the toxR regulon are essential for Vibrio cholerae pathogenesis in humans, *J. Exp. Med.*, 1988, **168**(4), 1487–1492.
5 M. K. Waldor and J. J. Mekalanos, Lysogenic conversion by a filamentous phage encoding cholera toxin, *Science*, 1996, **272**(5270), 1910–1914.
6 B. D. Spangler, Structure and function of cholera toxin and the related Escherichia coli heat-labile enterotoxin, *Microbiol. Rev.*, 1992, **56**(4), 622–647.
7 S. M. Faruque and J. J. Mekalanos, Pathogenicity islands and phages in Vibrio cholerae evolution, *Trends Microbiol.*, 2003, **11**(11), 505–510.
8 W. L. Ng and B. L. Bassler, Bacterial quorum-sensing network architectures, *Annu. Rev. Genet.*, 2009, **43**, 197–222.
9 B. K. Hammer and B. L. Bassler, Quorum sensing controls biofilm formation in Vibrio cholerae, *Mol. Microbiol.*, 2003, **50**(1), 101–104.
10 S. A. Jung, L. A. Hawver and W. L. Ng, Parallel quorum sensing signaling pathways in Vibrio cholerae, *Curr. Genet.*, 2016, **62**(2), 255–260.
11 A. Shariati, M. Arshadi, M. A. Khosrojerdi, M. Abedinzadeh, M. Ganjalishahi, A. Maleki, *et al.*, The resistance mechanisms of bacteria against ciprofloxacin and new approaches for enhancing the efficacy of this antibiotic, *Front. Public Health*, 2022, 10.
12 M. A. Ali, S. K. Mohanty, K. Elumalai, K. S. Nataraj, C. Ayyanna and S. Srinivasan, Pyridine derivatives as preferable scaffolds for the process of discovering new drugs, *Appl. Chem. Eng.*, 2023, **6**(2), DOI: 10.24294/ace.v6i2.2053.
13 M. Hema, S. A. Princy, V. Sridharan, P. Vinoth, P. B. P. Balamurugan and M. N. Sumana, Synergistic activity of quorum sensing inhibitor, pyrizine-2-carboxylic acid and antibiotics against multi-drug resistant V. cholerae, *RSC Adv.*, 2016, **6**(51), 45938–45946.
14 H. B. Sarveswari, S. Kalimuthu, K. Shanmugam, P. Neelakantan and A. P. Solomon, Exploration of Anti-infectives From Mangrove-Derived Micromonospora sp. RMA46 to Combat Vibrio cholerae Pathogenesis, *Front. Microbiol.*, 2020, 11.
15 A. G. Al-Bakri, G. Othman and Y. Bustanji, The assessment of the antibacterial and antifungal activities of aspirin, EDTA and aspirin-EDTA combination and their effectiveness as antibiofilm agents, *J. Appl. Microbiol.*, 2009, **107**(1), 280–286.
16 B. Qin and B. L. Bassler, Quorum-sensing control of matrix protein production drives fractal wrinkling and interfacial localization of Vibrio cholerae pellicles, *Nat. Commun.*, 2022, **13**(1), 6063.
17 P. C. ADHIKARI, C. RAYCHAUDHURI and S. N. CHATTERJEE, The Lysis of Cholera and El Tor Vibrios, *J. Gen. Microbiol.*, 1969, **59**(1), 91–95.
18 D. Samal, J. Turuk, S. R. Nayak, S. Pany, B. B. Pal and S. Pati, Genomic insights into the dynamic antibiotic resistance landscape of Vibrio cholerae during the Cholera outbreak 2022 in Odisha, India, *Sci. Rep.*, 2025, **15**(1), 1503.
19 A. Sajeevan, D. J. Andrew, T. N. Patra, A. P. Solomon and R. Dandela, Novel synthesis and anti-pathogenic properties of ensifentrine and its intermediates against *Pseudomonas aeruginosa*, *RSC Adv.*, 2025, **15**(17), 13053–13063.
20 I. Jahan, B. Ganbaatar, C. W. Lee, S. H. Shin and S. Yang, Antibacterial and antibiofilm features of mutSMAP-18 against Vibrio cholerae, *Heliyon*, 2024, **10**(21), e40108.
21 A. Potapova, W. Garvey, P. Dahl, S. Guo, Y. Chang, C. Schwechheimer, *et al.*, Outer membrane vesicles and the outer membrane protein OmpU govern *Vibrio cholerae* biofilm matrix assembly, *mBio*, 2024, **15**(2), e03304.
22 B. L. Fung and K. L. Visick, LitR and its quorum-sensing regulators modulate biofilm formation by *Vibrio fischeri*, *J. Bacteriol.*, 2025, **207**(2), e00476.
23 R. Shobana, J. H. Thahirunnisa, S. Sivaprakash, A. J. Amali, A. P. Solomon and D. Suresh, Effect of palladium(II) complexes on NorA efflux pump inhibition and resensitization of fluoroquinolone-resistant Staphylococcus aureus: *in vitro* and *in silico* approach, *Front. Cell. Infect. Microbiol.*, 2023, **13**, 1340135.
24 M. Heidary, A. Ebrahimi Samangani, A. Kargari, A. Kiani Nejad, I. Yashmi, M. Motahar, *et al.*, Mechanism of action, resistance, synergism, and clinical implications of azithromycin, *J. Clin. Lab. Anal.*, 2022, **36**(6), e24427.
25 R. S. Mohanraj and J. Mandal, Azithromycin can induce SOS response and horizontal gene transfer of SXT element in Vibrio cholerae, *Mol. Biol. Rep.*, 2022, **49**(6), 4737–4748.
26 D. Paul, M. Chawla, T. Ahrodia, L. Narendrakumar and B. Das, Antibiotic Potentiation as a Promising Strategy to Combat Macrolide Resistance in Bacterial Pathogens, *Antibiotics*, 2023, **12**(12), 1715.
27 P. Gupta, B. Mankere, S. C. Keloth, U. Tuteja and K. T. Chelvam, Persistence of V. cholerae O139 Biofilm Against Physical, Chemical and Antibiotic Lethal Challenges, *Proc. Natl. Acad. Sci. India B Biol. Sci.*, 2019, **89**(3), 1117–1124.
28 A. Meza-Villezcas, A. L. Gallego-Hernández, F. H. Yildiz, O. E. Jaime-Acuña, O. Raymond-Herrera and A. Huerta-Saquero, Effect of antimicrobial nanocomposites on Vibrio cholerae lifestyles: Pellicle biofilm, planktonic and surface-attached biofilm, *PLoS One*, 2019, **14**(6), e0217869.